NIH Public Access
Author Manuscript
Ultramicroscopy. Author manuscript; available in PMC 2012 December 1.

Published in final edited form as:
Ultramicroscopy. 2011 December ; 111(12): 1688–1695. doi:10.1016/j.ultramic.2011.09.015.

Design of a hybrid double-sideband/single-sideband (schlieren) objective aperture suitable for electron microscopy

Bart Buijsse[a], **Frank van Laarhoven**[a], **Andreas K. Schmid**[b], **Rossana Cambie**[b], **Stefano Cabrini**[b], **Jian Jin**[b], and **Robert M. Glaeser**[b,*]

[a]FEI Company, PO Box 80066, 5600 KA Eindhoven, The Netherlands [b]Lawrence Berkeley National Laboratory, University of California, Berkeley, CA 94720, USA

Abstract

A novel design is described for an aperture that blocks a half-plane of the electron diffraction pattern out to a desired scattering angle, and then – except for a narrow support beam – transmits all of the scattered electrons beyond that angle. Our proposed tulip-shaped design is thus a hybrid between the single-sideband (ssb) aperture, which blocks a full half-plane of the diffraction pattern, and the conventional (i.e. fully open) double-sideband (dsb) aperture. The benefits of this hybrid design include the fact that such an aperture allows one to obtain high-contrast images of weak-phase objects with the objective lens set to Scherzer defocus. We further demonstrate that such apertures can be fabricated from thin-foil materials by milling with a focused ion beam (FIB), and that such apertures are fully compatible with the requirements of imaging out to a resolution of at least 0.34 nm. As is known from earlier work with single-sideband apertures, however, the edge of such an aperture can introduce unwanted, electrostatic phase shifts due to charging. The principal requirement for using such an aperture in a routine data-collection mode is thus to discover appropriate materials, protocols for fabrication and processing, and conditions of use such that the hybrid aperture remains free of charging over long periods of time.

Keywords

Phase contrast; single-sideband aperture; charging

INTRODUCTION

Cryo-EM specimens of biological macromolecules [1] are well-approximated as weak phase objects, in the sense that the amount of amplitude contrast that is present is too faint to provide significant structural information. It is well known that images of phase objects show almost no contrast under ideal (diffraction-limited) imaging conditions [2]. It thus is standard practice to record cryo-EM images at rather high levels of defocus in order to provide sufficient contrast to recognize objects of interest. Defocus-based imaging nevertheless provides only a small fraction of the phase contrast that is, in principle,

© 2011 Elsevier B.V. All rights reserved.

*Corresponding author: Dr. Robert M. Glaeser, 363B Donner Laboratory, Lawrence Berkeley National Laboratory, University of California, Berkeley, CA 94720, Phone: 510-642-2905, FAX: 510-486-6488, rmglaeser@lbl.gov.

Publisher's Disclaimer: This is a PDF file of an unedited manuscript that has been accepted for publication. As a service to our customers we are providing this early version of the manuscript. The manuscript will undergo copyediting, typesetting, and review of the resulting proof before it is published in its final citable form. Please note that during the production process errors may be discovered which could affect the content, and all legal disclaimers that apply to the journal pertain.

NIH-PA Author Manuscript
NIH-PA Author Manuscript
NIH-PA Author Manuscript

NIH-PA Author Manuscript

NIH-PA Author Manuscript

NIH-PA Author Manuscript

available due to phase-modulations in the transmitted (exit) wave [3, 4]. In addition, defocus-based imaging introduces unwanted oscillations in the contrast transfer function (CTF). Recording images at high defocus also results in a significant loss of high-resolution signal due to both delocalization [5] and the focus-dependent, spatial-coherence envelope function [6].

A conceptually simple, alternative method for producing contrast in images of phase objects is to use a microfabricated objective-lens aperture to modify a half-plane of the scattered electron wave in a desirable way. One possibility is to use a thin carbon film to apply a phase shift of 180° to only one side of the scattered wave, thereby producing so-called Hilbert phase contrast [7,8]. A related possibility is to block one half of the scattered wave completely, thereby producing what is called “schlieren” contrast in light microscopy and other optical applications [9]. In electron microscopy, masking off a half plane of the diffraction pattern has been referred to as the “Foucault method”[10], and it has been said to produce “Foucault contrast” [10, 11] and optical shadowing [12], but it is more commonly said (in the context of electron microscopy) to produce single-sideband (ssb) contrast [6].

A useful feature of single-sideband contrast is the fact that all Fourier components are transferred with constant amplitude, i.e. without the oscillations associated with the defocus-based, double-sideband (dsb) CTF. As is described below, however, the amplitudes of the Fourier components are half of those in a Zernike phase-contrast image, and the phases are shifted by $(\frac{\pi}{2} - \gamma(s))$, where $\gamma(s)$ is the familiar wave aberration due to spherical aberration and defocus. In other words, the phase-distortion function associated with defocus and lens aberrations, as well as the 90° phase shift on scattering, show up as a combined (spatial-frequency dependent) phase shift, rather than producing oscillations in the CTF. As a result, it is desirable to record ssb images close to focus and with little or no other lens aberrations.

The option of single-sideband imaging has been given serious consideration in electron microscopy in the past [13–15]. Further development of the method did not continue, however, due to the difficulty that was experienced in preventing electrostatic charging of the aperture. Charging of the aperture produces unwanted phase shifts in the scattered wave function, of course, and – as was just mentioned – these phase shifts appear in the phases of the Fourier components of the image rather than in modulations of the CTF amplitude. The fact that one cannot easily tell whether the aperture is charging thus makes it particularly difficult to work with the single-sideband aperture. A further disadvantage of using a full half-plane version of the single-sideband aperture (even in the absence of charging) is the fact that one is not able to determine the defocus value of such images without taking a companion image, with the aperture removed, for which the CTF has the familiar focus-dependent oscillations.

We now propose a variant of the single-sideband aperture in which a half-plane of the scattered wave is blocked only at low spatial frequencies, while the intermediate and high spatial frequencies are still imaged with the familiar, double-sideband CTF. To explain the concept more clearly, a scanning electron microscope image is shown in Figure 1A, where one can see the tulip-shaped feature that is introduced into the otherwise open objective aperture. This design of single-sideband aperture overcomes some of the disadvantages described above, while still retaining the important feature that the low-frequency Fourier components are imaged with much greater contrast than is possible with a fully open (i.e. double-sideband) aperture, even at high defocus.

In a preferred implementation, illustrated by the theoretical CTF shown in Figure 1B, one would aim to record images at Scherzer defocus, and the radius of the opaque, half circle would correspond to the point at which the dsb CTF first rises to a value of 0.5. The full CTF would thus start at a constant value of 0.5 at a cut-on frequency that depends upon how

NIH-PA Author Manuscript

NIH-PA Author Manuscript

NIH-PA Author Manuscript

close one brings the edge of the aperture to the unscattered beam. The amplitude of the CTF would then remain at a value of 0.5 out to the spatial frequency where double-sideband imaging would first begin, after which the CTF would soon rise to values close to 1.0, staying there until the point where oscillations of the CTF first begin.

When using the hybrid dsb/ssb aperture, and contrary to the situation when using a full (i.e. half-plane) ssb aperture, unwanted phase shifts due to charging are manifested as distortions of the Thon rings (i.e. oscillations in the CTF) that now remain in the dsb portion of the aperture. These oscillations also allow for determination of the image defocus, without requiring that one take a second image with the aperture retracted.

In the current work, we demonstrate that the hybrid double-sideband/single-sideband (dsb/ssb) aperture can be fabricated from thin-foil materials by using the technology of focused-ion beam (FIB) milling. We also present initial experiments to demonstrate the proof-of-concept of hybrid dsb/ssb contrast transfer. While such hybrid dsb/ssb apertures currently remain sensitive to charging, the advantages of this design may be sufficiently great to warrant a renewed effort to find materials, fabrication protocols, and conditions of use that fully overcome the problem of charging.

MATERIALS AND METHODS

Fabrication and surface-characterization of apertures

Experimental hybrid dsb/ssb apertures were fabricated from thin metal foils (described below) both at FEI Company, using a Helios 400 DualBeam system (SEM/FIB), and at the LBNL Molecular Foundry, using a Zeiss model XB1540 CrossBeam® workstation. The surfaces of representative devices were characterized by X-ray photoeletron spectroscopy (XPS), using either a Quantra SXM from Ulvac-PHI at Philips Research Eindhoven or a PHI 5400 (Physical Electronics, Inc.) tool at the Molecular Foundry.

Apertures made from a 1 μm-thick molybdenum foil were fabricated, characterized by XPS, and evaluated by electron microscopy in Eindhoven. No steps were taken to remove native oxide (if any) or to remove gallium that could have been deposited during milling with the FIB. Surface analysis of representative devices by XPS indicated that they were coated with a 1 nm-thick surface layer containing substantial organics as well as oxygen, with less than 1 % molybdenum detectable by this method of analysis.

Apertures made from 5 μm-thick, 5N (i.e. 99.999 percent pure) gold foil were fabricated, characterized by XPS, and evaluated by electron microscopy in Berkeley. The 5N gold foil was purchased from ESPI Metals (Ashland, OR). All devices were cleaned by argon sputtering while in the XPS tool in order to remove carbon, oxygen, and the residual gallium that was easily detected after milling in the FIB. Surface analysis by XPS showed that exposure of devices to ambient atmosphere quickly resulted in a surface composition that once again was roughly 1/3 Au, 1/3 C, and 1/3 O, even though Au was the only detectable element after the previous cleaning step.

Electron microscopy

The image quality obtained when using hybrid dsb/ssb apertures was determined by evaluating the appearance of Fourier transforms of images of commercially available test specimens. In some cases our experiments used holey carbon films onto which graphitized-carbon particles were deposited, and in other cases we used gold-shadowed carbon replicas of an optical-diffraction grating. The primary goal, when using either specimen, was to evaluate whether unwanted distortions could be detected in the contrast transfer function (CTF), i.e. the Thon rings that are readily seen for amorphous carbon films. Distortion, if

NIH-PA Author Manuscript

NIH-PA Author Manuscript

NIH-PA Author Manuscript

any, of the Thon rings can only be due to unwanted distortions in the electrostatic and magnetic field that are associated with the aperture. Specimens containing graphitized carbon particles also proved to be valuable in determining whether images retained significant signal at a resolution of 0.34 nm.

Experiments at Eindhoven were performed with a standard FEI Tecnai F20 electron microscope, operated at an energy of 200 keV. In this case the microfabricated apertures were inserted into the back focal plane of the objective lens, using an aperture holder that was modified only to allow heating of the aperture, if desired. Images were recorded on a Gatan Multiscan CCD camera (model 794).

Experiments at Berkeley were performed with a modified (low-base) FEI Titan 80–300 electron microscope, operated at an energy of 300 keV. The modifications provided in this instrument include relay optics that magnify the electron diffraction pattern by a factor of ~6 at a plane that exists within the section of the column that, in other applications, is used to house an aberration corrector. Three (2.5 cm-diameter) ports are provided in this instrument to allow for insertion of a phase-plate aperture holder as well as additional experimental apparatus, such as an anticontaminator. In this case the microfabricated apertures were inserted into the plane of the magnified image of the electron diffraction pattern, using a home-built aperture holder that can be heated to a temperature of 400° C. Images were recorded on a 2kx2k FEI Eagle CCD camera.

THEORY OF IMAGE FORMATION AND RESTORATION

A mathematical description of image formation when using a single-sideband aperture, which considers only one Fourier component at a time, is given in [6], and a more detailed exposition is given in the supporting material of [16]. The same mathematical approach was used previously by Downing and Siegel, who wrote the results for a combined weak-phase, weak-amplitude object as an integral over the open area of the aperture [15]. This simple derivation has the virtue that it provides a transparent explanation of why the amplitude of the CTF is 0.5, independent of the defocus or the spatial frequency (compare, for example, Equations S9 and S11). In addition, it clearly explains why the sinusoidal fringes, formed by interference of a single diffracted beam with the unscattered beam, shift their phase origin as the focus is changed.

An alternative derivation can be used in which the image intensity is represented in closed form rather than as a continuous sum (integral) over a distribution of spatial frequencies. In this approach the opaque half-plane aperture is represented by the Heaviside step function, the definition of which is given in equation S1. In Goodman [17], for example, the reader is guided through such a derivation while working problem 7-3. For convenience, we also provide a step-by-step derivation in the supplemental material. The closed-form result is instructive in that the image wave function is represented as the convolution of the exit wave (i.e. the wave transmitted through the specimen) and the (coherent wave) point-spread function for the objective lens. In the case of a diffraction-limited image, the (coherent wave) point-spread function is the Fourier transform of the Heaviside function (see equation S3).

As is shown in the derivation of equation S6, when the straight edge of the Heaviside function is perpendicular to the *x*-axis, the single-sideband image intensity for a weak phase object is proportional to

$$I(x,y)=1+2\sigma V'(x,y)\otimes\Im^{-1}sin\,\gamma(s_x,s_y)+\left(2\sigma V'(x,y)\otimes\Im^{-1}cos\,\gamma(s_x,s_y)\right)\otimes\frac{1}{\pi x}, \quad \text{Equation 1}$$

NIH-PA Author Manuscript

NIH-PA Author Manuscript

NIH-PA Author Manuscript

where σ is the coupling constant for elastic scattering (i.e. $\sigma = \frac{2\pi}{hv}$, where h is Planck's constant and v is the electron velocity), $V'(x,y)$ is the projection of the shielded coulomb potential of the object, and $\gamma(s)$ is the familiar wave aberration function due to spherical aberration and defocus. Note that no loss in generality is incurred by suppressing, here, the factor of 4 that is present on the left-hand side of equation S6. This proportionality constant derives from the mathematical definition of the Heaviside function that is given in equation S1, where the amplitude of the unscattered beam (i.e. $s = 0$) is mathematically modeled as having a value of ½, resulting in an average intensity that is reduced by a factor of 4. In practice, of course, the unscattered beam will not be attenuated by an experimentally realizable approximation to the Heaviside function.

A crucial point that is expressed in equation 1 is the fact that using a single-sideband (Heaviside function) aperture introduces a term, in the image contrast, in which phase modulations in the exit wave function are converted, by way of a $\cos\gamma$ transfer function, into amplitude modulations in the image intensity. The single-sideband (Heaviside) filter thus has an effect similar to that of a Zernike phase plate. Unlike the Zernike phase plate, however, this term is convoluted with the one-dimensional function, $\frac{1}{\pi x}$, which is responsible for the "optical shadowing" effect described in the Introduction. This shadowing effect is further illustrated in the simulated images of Gaussian spheres that are shown in Figure S1.

The Fourier transform of the image intensity produced when using a single-sideband aperture is more easily understood from the perspective of an alternative derivation, mentioned above, in which each Fourier component of the exit wave produces only one scattered beam that passes through the aperture, while its Friedel mate is blocked by the aperture. This "solitary" scattered beam then interferes with the unscattered beam, producing a sinusoidal interference fringe. In this case the phase distortion due to defocus (if any) and lens aberrations appears as a systematic error in the phases of the structure factor of the object[6], rather than as a focus-dependent modulation of the contrast-transfer function.

Due to the effects just described, it is necessary to computationally correct the systematic distortions that occur in single-sideband images, just as one must apply a CTF correction to the data obtained in defocused dsb images. To understand what corrections should be made, we begin by noting that – apart from an arbitrary scale factor – the Fourier transform of the singleside-band image intensity, which we rewrite here from Equation S9, is

$$\Im\left\{I_{single-sidebandimage}(x,y)\right\} = \delta(s_x, s_y) + i\sigma\tilde{F}(s_x, s_y)\cdot sgn(s_x), \qquad \text{Equation 2}$$

where $\tilde{F}(s_x, s_y) = F(s_x, s_y)e^{i(\alpha(s_x, s_y)-\gamma(s))}$ is the Fourier transform of the projected Coulomb potential, $V'(x,y)$. Equation 2 thus makes it clear that that first step is to simply apply a phase shift of $\frac{\pi}{2}$ to all Fourier components of the image intensity, other than the origin. The second step is to change the sign of all Fourier components in the "negative" half-plane, and the third step is to undo the systematic phase error in the structure factor, which is due to defocus and lens aberrations. The final step is to do an inverse Fourier transform using the restored structure factors.

In the case of the hybrid dsb/ssb aperture described in the current work, this restoration algorithm applies only to the single-sideband portion of the diffraction pattern. The values of the Fourier transform at spatial frequencies lying within the dsb part of the aperture remain

NIH-PA Author Manuscript

NIH-PA Author Manuscript

NIH-PA Author Manuscript

identical to the corresponding values obtained when using a completely open (i.e. conventional) objective-lens aperture. Image restoration for the dsb frequencies would thus be done by the same CTF correction that one would normally use for images recorded with a fully open objective aperture.

Since the contrast in the single-sideband portion of the Fourier transform is half that of the (maximum) contrast in the double-sideband portion (compare equations S9 and S11), it is recommended to put the two portions on the same scale by doubling the magnitudes of the single-sideband Fourier components. The rationale is similar to that in which high-resolution Fourier components (of conventional, double-sideband images) are frequently boosted by "an inverse B-factor" to compensate for the steeply decaying MTF of the detector, among other factors.

RESULTS

The best results to date have been obtained with devices fabricated from thin molybdenum foil. The results obtained with such devices approach but do not fully reach the theoretically expected level of performance, as is shown in Figure 2. After correcting the astigmatism, the Thon rings in the dsb part of the spectra remain circular at all values of defocus tested. In addition, the amplitude in the ssb part of the spectra remains constant, independent of the amount of defocus. As is expected, the point of transition between the dsb and ssb portions of the power spectrum is clearly visible when the value of the CTF for a dsb image is either smaller (Figure 2A) or greater (Figure 2C) than 0.5, but the ssb portion appears to merge continuously with the dsb portion when the value of the dsb CTF is close to 0.5 at the boundary between the two (Figure 2B). Even so, the radial positions of the zeros in the CTF do not fall accurately at the expected positions, even when using a value of defocus that gives a best fit between theory and experiment.

The results shown in Figure 3 illustrate a number of other features of interest. When images of a nearly-transparent particle of graphitized carbon are recorded close to focus, for example, there is more contrast for the low-resolution features in the image recorded with the hybrid aperture (Figure 3A) than in the image recorded without such an aperture (Figure 3B). (In the latter case, removal of the single-sideband aperture was approximated by moving the edge of the ssb half-circle far away from the center of the electron diffraction pattern.) At the same time, the graphitized-carbon particle shows a significant amount of amplitude contrast, and, in addition, we believe that the very dark portions of the particle in Figure 3 (most notably along the lower right-hand edge of the particle) may be due to particularly strong phase shifts in the exit wave for that area of the particle. While both effects are non-ideal for the current purpose, the usefulness of this test specimen for evaluating distortions in the Thon rings and for evaluating the retention of information at a resolution of 0.34 nm has made it desirable to use for our initial work.

The image recorded with the edge of the ssb aperture close to the unscattered beam (Figure 3A) shows a degree of optical shadowing [12] or edge enhancement – both for the particle and for the hole in the carbon film, as is expected from theory (see equation 1 and the accompanying narrative). In addition, the image recorded with the edge of the ssb aperture close to the unscattered beam shows a halo or fringe both at the edge of the particle and at the edge of a hole in the carbon film, as do Zernike phase-contrast images. In both cases it is believed that the halo (fringe) is due to the fact that the edge of the aperture cannot be placed arbitrarily close to the zero-frequency Fourier component of the exit wave. Thus, unlike the theoretically idealized case described in equation 1, there is a gap of spatial frequencies between the unscattered beam and the edge of the device. In other words there is a non-zero cut-on frequency at which the Fourier components of the image abruptly switch from weak,

NIH-PA Author Manuscript

NIH-PA Author Manuscript

NIH-PA Author Manuscript

double-sideband (mainly amplitude) contrast to strong, single-sideband (predominantly phase) contrast.

Figure 3C shows the computed Fourier transform of the image presented in Figure 3A. Of particular interest in this case is the fact that diffraction spots from the 0.34 nm lattice planes of the graphitized carbon particle are visible in all directions. This result demonstrates that – as expected – there is no inherent limitation in the image resolution caused by using the hybrid dsb/ssb aperture, at least out to the highest resolution that is currently achieved in cryo-EM of single particles.

Figure 3D, on the other hand, which shows the computed Fourier transform of Figure 3B, demonstrates that electrostatic charging is present along the straight edge of the opaque half-circle. Charging of the device is evident, in the first instance, from the presence of a thin line of anomalous contrast-transfer close to the edge, and, in the second instance, from the distortion of the previously circular first maximum of the CTF. The degree of charging seen in Figure 3D develops within a period of 5 – 10 minutes, when the total beam current is 0.5 nA, and it becomes progressively worse, the longer the device is exposed to the electron beam.

On closer analysis of Figure 2 and Figure 3C, there is also evidence of charging of the aperture when the straight edge of the opaque half circle is close to the unscattered beam. Although the Thon rings show very little distortion from the circular shape expected in the absence of charging, the zeros do not occur at the radial positions (spatial frequencies) that they would do if spherical aberration and defocus were the only factors contributing to the phase shift in the back focal plane (as we noted above). The same effect is seen with thin-carbon phase plates when they exhibit charging[18].

We have found that charging of the Mo device is not reduced when the aperture is heated. While heating should reduce the risk of carbonaceous contamination, it may increase the risk of forming a surface oxide and the risk of migration of contaminants from the bulk to the surface of the metal foil. In any event, heating the Mo device is not currently a viable way to prevent charging effects.

Finally, the computed Fourier transform in Figure 3D shows that diffraction from the 0.34 nm lattice planes of the graphitized carbon particle is no longer present in all directions when the ssb part of the aperture is moved out into the intermediate-resolution part of the diffraction pattern. Although we suspect that the loss of resolution, which is in the same direction that the aperture was moved, may be due to rapid fluctuations in the amount of charging of the edge of the aperture, it remains still to be determined whether that is the correct explanation.

We have also done numerous experiments with devices fabricated from gold, but in this case charging has proven to be even more of a challenge than it is for molybdenum. As with the Mo device, apertures that we have made from Au often showed more severe charging effects when heated than they do at room temperature. Thin-foil devices made by evaporating gold into the trenches of a mold, which was formed by photolithography, showed considerable charging right from the beginning, i.e. both before and after heating. Thin-foil devices made by electroplating gold have been found to be even worse in that regard.

Much better results were obtained, on the other hand, with devices fabricated from either 25 μm-thick or 5 μm-thick, 5N Au foil by ion milling with a FIB. When used initially at room temperature, such devices showed little or no detectable charging along straight-cut edges of a rectangular-shaped test-device. Significant charging was still present at corners, however, both concave and convex in shape, an effect that did not appear to happen with devices that

NIH-PA Author Manuscript

NIH-PA Author Manuscript

NIH-PA Author Manuscript

were fabricated from the thinner, Mo foil. When heated to a temperature as low as 185° C, however, the same Au devices immediately showed quite severe charging effects along straight-cut edges, an example of which is shown in Figure 4. This high level of charging then persisted when the same device was again cooled to room temperature

The onset of charging, which occured when the gold foil was heated, was also accompanied by the appearance of trace amounts of contamination on the surface of the foil. XPS analysis of the surface of a heated device showed the presence of small peaks that were not there in the final, cleaned device, prior to heating. We do not yet know whether these contaminants migrated to the surface from within the bulk of the 5N foil (presumably from material at the grain boundaries rather than material dissolved within the gold itself) due to thermal annealing, or whether they arrived by surface diffusion from materials in the aperture holder.

DISCUSSION

Key features of the hybrid dsb/ssb aperture

The tulip (hybrid dsb/ssb) aperture has certain features that could make it a good choice for imaging cryo-EM specimens and other weak-phase objects. It is not necessary, for example, to use an objective lens with a longer focal length than usual in order to realize a sufficiently low cut-on frequency, as currently is the case for Zernike phase plates. Instead, the user can simply bring the straight edge of the ssb part of the aperture as close as desired to the unscattered beam of the electron diffraction pattern. It is thus possible for such an aperture to be used in existing electron microscopes. It may be necessary, however, to use a modified objective aperture rod that allows more precise positioning than can be conveniently achieved with standard aperture rods. In addition, it is not yet known what modifications of the aperture rod, such as heating or cooling, may be needed to minimize charging. Furthermore, provision of an airlock system would facilitate rapid replacement of contaminated apertures, something that may prove to be important for phase-contrast apertures. Even so, the hybrid dsb/ssb aperture has the potential to be a relatively inexpensive and widely accessible option for achieving greatly improved CTF properties when imaging weak phase objects.

Another motivation for development of the hybrid dsb/ssb aperture is that there is a much wider range of materials from which such an aperture can be fabricated than is the case for the thin-foil, Zernike-type phase contrast aperture. As an example, it is hoped that the hybrid dsb/ssb aperture can be fabricated from materials that do not suffer from the aging effect, which currently limits the useful lifetime of the thin carbon-film phase plate [19].

There are, at the same time, certain disadvantages of using the hybrid dsb/ssb aperture rather than a Zernike phase plate. The amount of phase contrast is not adjustable for the dsb/ssb aperture, as it is for an electrostatic phase plate. In addition, the amount of contrast at low resolution is only half of what can be produced with a Zernike plate. Even so, the substantial increase in low-resolution contrast that is expected when using a dsb/ssb aperture may well be more than enough for many applications, while the full amount of phase contrast is still retained within the high-resolution band pass of Scherzer defocus.

Image restoration (CTF correction) is still required with the dsb/ssb aperture

Computational image restoration (discussed in the Theory section above) is required when applying a Heaviside step-function filter in Fourier space. One must correct the systematic phase errors that are due to defocus (if any) and lens aberrations, as well as undo the optical shadowing effect that is introduced by such an aperture. This image restoration operation is nevertheless arguably less likely to cause errors than is the currently required CTF correction. For example, there are no zeros in the CTF that one must deal with, and, in

NIH-PA Author Manuscript

NIH-PA Author Manuscript

NIH-PA Author Manuscript

addition, the images can be recorded with little or no defocus. Even so, Zernike phase plates and the ssb aperture both apply a sharp cut-on, which – as is mentioned above – is expected to generate a halo or fringe at the edge of a particle. Many users thus may want, in both cases, to preprocess their data in order to minimize this effect, as was done recently by Danev et al. [20, 21].

It is worth mentioning that separate images of the amplitude modulations and of the phase modulations in the exit wave of a weak object can be recovered from the sum and from the difference, respectively of the image intensities recorded with two oppositely facing ssb apertures [15]. An equivalent recovery of amplitude and phase modulations for strong objects, not discussed here, however, is necessarily more complex.

Charging of metal apertures

At the moment, all types of microfabricated dsb/ssb apertures are prone to show charging effects that are detectable in the form of distortions of Thon rings and/or as an anomalous glow of contrast at the edge of a device. As a result, we believe that electrostatic charging of microfabricated devices is the single, most important challenge that must be addressed for further development of such apertures.

The charging referred to here can even become apparent well before the focused beam touches the edge of the device. It thus seems unlikely – although not completely ruled out – that this initial charging effect is caused by the build-up of carbon-rich contamination, such as that which is seen on specimens when irradiated with the beam at crossover, or on specimens imaged in an SEM at high magnification. On the other hand, we can add that we do see a localized, further increase in charging when the focused electron beam is allowed to touch the edge of a room-temperature device for many 10s of seconds. We believe that this increased charging is, indeed, due to the buildup of a spot of carbon-based contamination.

From a theoretical (physical) point of view, we believe that the charging encountered with metal devices is necessarily limited to formation of a surface-distribution of electrostatic dipoles, rather than to some net amount of (uncompensated) surface-charge. There can be many situations, of course, in which immobile charges are trapped on the surface of a metal device, including the case where there is a native oxide layer on the surface, or the case when carbon-rich contamination builds up in areas that are hit by the focused electron beam. In all such cases, however, one expects that the immobile charge will be compensated by equal and opposite (image) charges within the underlying conductor. The build up of a significant amount of uncompensated, net charge can only be expected to occur when the entire device, and not just a thin surface layer, is an electrical insulator, or when the device is isolated from ground by an open circuit. We thus do not expect that there can be a significant Coulombic (i.e. net charge) contribution to the electrostatic potential within the area of the aperture.

Interestingly, it was once thought that placing an insulating probe (experiments described in[11]) or fiber [22] at, or close to, the unscattered beam would be an effective way to introduce phase contrast. However, as one knows from experience with bare plastic sections, or when an unwanted piece of lint gets into the microscope column, the charging effects that occur with isolated insulators are quite severe and uncontrollable.

It is important to discuss the fact that the contact potential between different materials is almost certain to cause an accumulation of net charge on an aperture, even before it is hit by the electron beam. A net transfer of electrons must occur between the aperture and any surrounding metal to which it is electrically connected, if the two are made of different materials. As a result, one can expect there to be a spatially varying electrostatic potential in

NIH-PA Author Manuscript

NIH-PA Author Manuscript

NIH-PA Author Manuscript

the open area between the objective aperture and the surrounding metal, whose isopotential surfaces are affected by the shape of the microfabricated device. We believe, however, that the effect of the contact-potential on the Thon rings will be negligible in the case of a microfabricated dsb/ssb aperture, as it is for a normal, circular aperture. Nevertheless, we performed an experiment to specifically test whether biasing a dsb/ssb aperture by a fraction of a volt would cause a noticeable change in the Thon rings. The result was, as we had expected, that we did not see any change in the Thon rings, even when the bias voltage was varied between 20 and 400 millivolts. In our ongoing experiments with a drift-tube phase plate [23], for comparison, we have determined experimentally that a bias of 20 mV applied to a 5 μm long drift tube produces a 90-degree phase shift for 80 keV electrons.

Local “patch-field” effects might be responsible for the observed charging of metallic devices

As we mentioned above, we currently believe that the charging effects observed with our metallic devices are due to a distribution of locally compensated surface charges, e.g. dipole sheets whose dipole moment per unit area may vary over the surface of a device. There are, in fact, many possibilities for ways in which this type of charging of a metal device can occur. One possibility, mentioned previously, is that there may be a native oxide layer on the surface of the metal that becomes charged when hit by scattered electrons, let alone the much stronger, unscattered beam, or that organic contaminants on the surface become polymerized when hit by the focused, unscattered electron beam. In both cases, of course, the insulating layer must be thick enough that it can hold a charge, rather than for the surface charge to be immediately neutralized by electron-tunneling to or from the underlying metal. Other possibilities that we are not able to exclude at present include variations in the work function of different facets of a pristine, crystalline material; local variations in the work function due to physisorption or chemisorption of impurities, and even variations in the extent to which different metal grains are doped by impurities.

The increased charging that is seen when devices are heated may be due to significant growth in the grain size, especially in the case of devices made from gold. The concern in this case is that patchy variations in the potential at the surface of a device, due to variations in work function, will extend for greater distances out into the open area of the aperture, the larger the grain size. Other reasons why heating might increase the amount of charging can include an increased tendency to form oxide, especially for Mo but even for Au, or migration of impurities from the bulk (or from surrounding materials) to the surface of a device as a result of heating, as was observed by XPS analysis even for a foil of 5N gold.

Charging should be preventable, once the root-cause mechanism is identified

The formation of a surface oxide, due, for example, to chemical reaction with molecular oxygen or water at high temperature, may be difficult to prevent. The same is true for oxidation of the surface due to ionization and reactive dissociation of adsorbed water that can occur when the metal surface is hit by electrons. One possibility for avoiding oxidation may nevertheless be to introduce a small leak of H_2 in order to reduce the oxide as quickly as it is formed.

Increases in the sizes of individual crystalline domains of gold during annealing (i.e. heating) may also be difficult to prevent. An alternative strategy for preventing the buildup of polymerized organic materials may thus be to cool the aperture in order to stop surface diffusion, which is known to be the primary route by which additional contaminant molecules are added to a spot of contamination. Migration of impurities from the bulk to the surface might also be avoided by using cooling rather than heating as a way to prevent the build up of carbon-based contamination.

NIH-PA Author Manuscript

NIH-PA Author Manuscript

NIH-PA Author Manuscript

If variation of the work function for different facets presented by individual crystalline domains is found to be a limiting factor, the problem should be solved by adding a processing step to reduce the grain sizes at the surface of a device, or even to create an amorphous structure at the surface. Ion milling in a FIB and sputter-cleaning with argon are both believed to have such an effect. As mentioned in the previous paragraph, it is likely that cooling the aperture would again have to be adopted as the approach to prevent the buildup of polymerized organic contamination, in order to avoid once again forming large metal grains by thermal annealing of the surface.

CONCLUSIONS

The tulip (hybrid dsb/ssb) design of an objective aperture produces single-sideband contrast at low spatial frequencies while retaining double-sideband contrast at high spatial frequencies. This design of a phase-contrast aperture has a number of advantages for imaging of weak phase objects. Such an aperture does not require the use of a special, longer focal length for the objective lens, as is currently required for thin carbon-film phase plates and for microfabricated, electrostatic phase plates. As a result, the hybrid dsb/ssb aperture may be used in an existing electron microscope, as was done for many of the experiments reported here. Furthermore, while a form of CTF correction is still required when using a hybrid dsb/ssb aperture, cryo-EM images can be taken much closer to focus, preferably at Scherzer defocus. This means that the loss of signal at high resolution, which occurs in highly defocused images due both to delocalization and to the spatial-coherence envelope function, will be far less with the hybrid aperture.

As is shown by proof-of-concept experiments reported here, the image quality achieved for intermediate-resolution and high-resolution spatial frequencies, i.e. in the double-sideband part of the Fourier spectrum, can be similar to that of images recorded with a conventional, fully open objective aperture. Nevertheless, our experiments also show that charging of the edge of the aperture that is closest to the center of the electron diffraction pattern remains a limitation, and that further work is required in order to overcome this problem. We believe, however, that the potential usefulness of the hybrid dsb/ssb aperture warrants the further development that is still needed in order to fully overcome the charging issue.

Supplementary Material

Refer to Web version on PubMed Central for supplementary material.

Acknowledgments

FEI Company obtained partial funding for this work through the innovation program Point One, which is carried out by AgentschapNL by order of the Dutch Ministry of Economic Affairs. This work was also supported in part by NIH grant GM083039 and in part through ENIGMA, a Scientific Focus Area Program supported by the US Department of Energy, Office of Science, Office of Biological and Environmental Research, Genomics: GTL Foundational Science through contract DE-AC02-05CH11231 between Lawrence Berkeley National Laboratory and the U.S. Department of Energy.

REFERENCES

1. Taylor KA, Glaeser RM. Retrospective on the early development of cryoelectron microscopy of macromolecules and a prospective on opportunities for the future. Journal of Structural Biology. 2008; 163:214–223. [PubMed: 18606231]
2. Zernike F. How I discovered phase contrast. Science. 1955; 121:345–349. [PubMed: 13237991]
3. Chang WH, et al. Zernike Phase Plate Cryoelectron Microscopy Facilitates Single Particle Analysis of Unstained Asymmetric Protein Complexes. Structure. 2010; 18:17–27. [PubMed: 20152149]

NIH-PA Author Manuscript

NIH-PA Author Manuscript

NIH-PA Author Manuscript

4. Hall RJ, Nogales E, Glaeser RM. Accurate modeling of single-particle cryo-EM images quantitates the benefits expected from using Zernike phase contrast. Journal of Structural Biology. 2011; 174:468–475. [PubMed: 21463690]
5. Downing KH, Glaeser RM. Restoration of weak phase-contrast images recorded with a high degree of defocus: The "twin image" problem associated with CTF correction. Ultramicroscopy. 2008; 108:921–928. [PubMed: 18508199]
6. Glaeser, RM.; Downing, K.; DeRosier, D.; Chiu, W.; Frank, J. Electron crystallography of biological macromolecules. Oxford University Press; 2007.
7. Nagayama K. Development of phase plates for electron microscopes and their biological application. European Biophysics Journal with Biophysics Letters. 2008; 37:345–358. [PubMed: 18259741]
8. Danev R, Nagayama K. Complex observation in electron microscopy: IV. Reconstruction of complex object wave from conventional and half plane phase plate image pair. Journal of the Physical Society of Japan. 2004; 73:2718–2724.
9. Settles, GS. Schlieren and shadowgraph techniques : visualizing phenomena in transparent media. Berlin; New York: Springer; 2001.
10. Cullis AG, Maher DM. Topological contrast in transmission electron microscope OPOGRAPHICAL CONTRAST IN TRANSMISSION ELECTRON-MICROSCOPE. Ultramicroscopy. 1975; 1:97–112. [PubMed: 1236033]
11. Grivet, P. Electron optics. Oxford; New York: Pergamon Press; 1965.
12. Haydon GB, Lemons RA. Optical shadowing in the electron microscope. Journal of Microscopy-Oxford. 1972; 95:483–&.
13. Downing KH. Possibilities of Heavy-Atom Discrimination Using Single-Sideband Techniques. Ultramicroscopy. 1979; 4:13–31.
14. Downing KH, Siegel BM. Phase-shift determination in single-sideband holography. Optik. 1973; 38:21–28.
15. Downing KH, Siegel BM. Discrimination of Heavy and Light Components in Electron-Microscopy Using Single-Sideband Holographic Techniques. Optik. 1975; 42:155–175.
16. Glaeser RM, Typke D, Tiemeijer PC, Pulokas J, Cheng A. Precise beam-tilt alignment and collimation are required to minimize the phase error associated with coma in high-resolution cryo-EM. Journal of Structural Biology. 2011; 174:1–10. [PubMed: 21182964]
17. Goodman, JW. Introduction to Fourier optics. San Francisco: McGraw-Hill; 1968.
18. Marko M, Leith A, Hsieh C, Danev R. Retrofit implementation of Zernike phase plate imaging for cryo-TEM. Journal of Structural Biology. 2011; 174:400–412. [PubMed: 21272647]
19. Danev R, Glaeser RM, Nagayama K. Practical factors affecting the performance of a thin-film phase plate for transmission electron microscopy. Ultramicroscopy. 2009; 109:312–325. [PubMed: 19157711]
20. Danev R, Kanamaru S, Marko M, Nagayama K. Zernike phase contrast cryoelectron tomography. Journal of Structural Biology. 2010; 171:174–181. [PubMed: 20350600]
21. Danev R, Nagayama K. Optimizing the phase shift and the cut-on periodicity of phase plates for TEM. Ultramicroscopy. In Press, Corrected Proof.
22. Unwin PNT, Klug A. Electron microscopy of stacked disk aggregate of tobacco mosaic virus protein. 1. 3-dimensional image reconstruction. Journal of Molecular Biology. 1974; 87:641–650. [PubMed: 4427373]
23. Cambie R, Downing KH, Typke D, Glaeser RM, Jin J. Design of a microfabricated, two-electrode phase-contrast element suitable for electron microscopy. Ultramicroscopy. 2007; 107:329–339. [PubMed: 17079082]

NIH-PA Author Manuscript
NIH-PA Author Manuscript
NIH-PA Author Manuscript

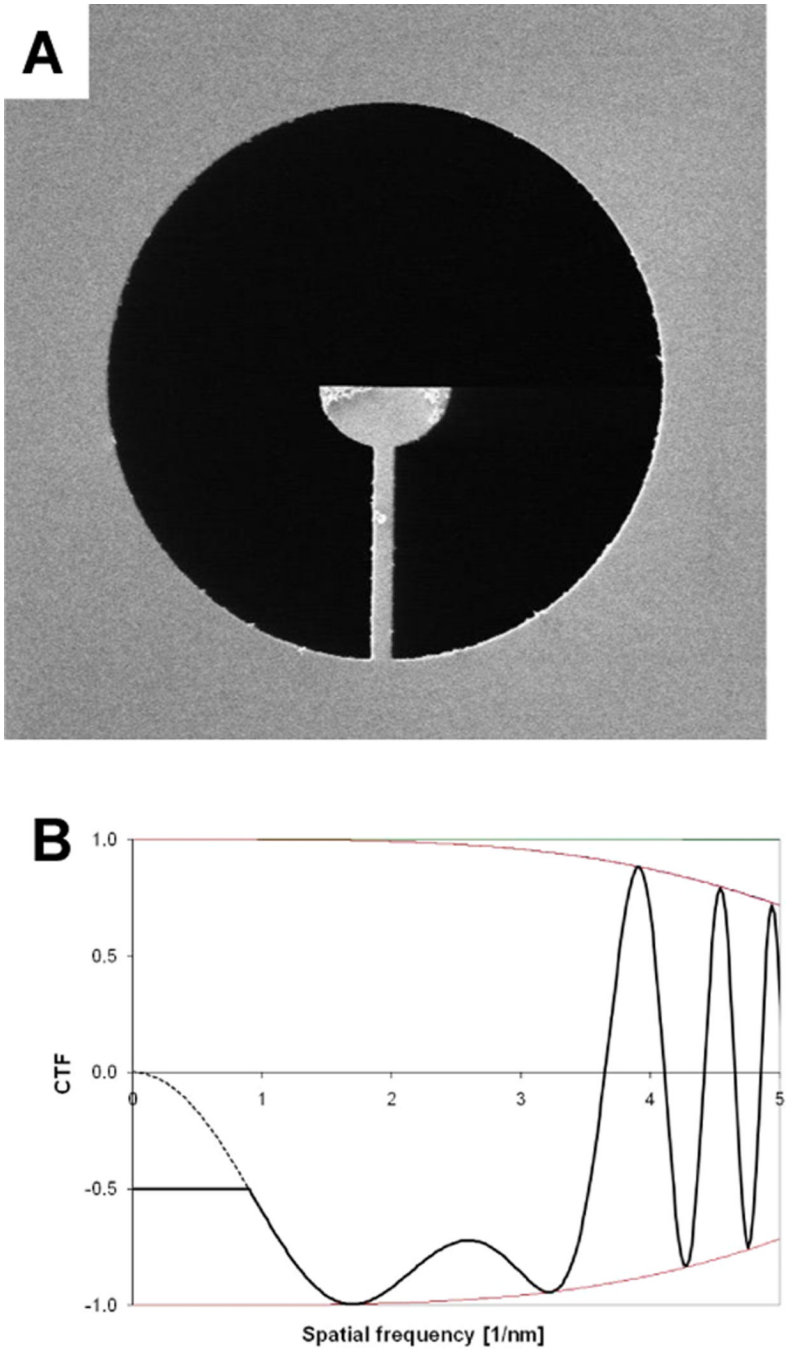

Figure 1.

Basic concept of the hybrid dsb/ssb aperture. (A) SEM image of a dsb/ssb aperture fabricated from a 1 μm-thick molybdenum foil by milling with a focused ion beam. The aperture diameter is 50 μm. When the electron-opaque half circle is positioned as closely as possible to the unscattered electron beam in an electron diffraction pattern, one half of the scattered wave will be blocked by the aperture, but only up to a scattering angle defined by the radius of the half circle. Beyond that, the device behaves as a fully open (double-sideband) aperture, apart from the unavoidable support beam that is seen in this image. (B) Comparison of CTF functions at Scherzer defocus for the hybrid dsb/ssb aperture and the usual, dsb aperture. The parameters used for this example are: electron energy = 200 keV,

NIH-PA Author Manuscript

NIH-PA Author Manuscript

NIH-PA Author Manuscript

energy spread = 0.8 eV, Cs = Cc = 2.1mm, illumination angle = 7.5×10^{-6} radian, and underfocus value = 88nm (Scherzer defocus). The envelope function is mainly due to partial temporal coherence in this case, and partial spatial coherence has little effect at this value of defocus. The CTF curve for images recorded with a hybrid dsb/ssb aperture is represented by the solid line, which is constant and equal to 0.5 at low resolution, and which switches to the same curve that applies to the dsb aperture when the latter first rises to a value of 0.5. For comparison, the CTF for images recorded with a fully open (dsb) aperture is represented by a dotted curve at spatial frequencies below the radius of the opaque half-circle of the ssb device. As is explained in the text, the CTF correction needed for images recorded with a hybrid dsb/ssb aperture is mathematically different for the single-sideband region than it is for the double-sideband region.

NIH-PA Author Manuscript
NIH-PA Author Manuscript
NIH-PA Author Manuscript

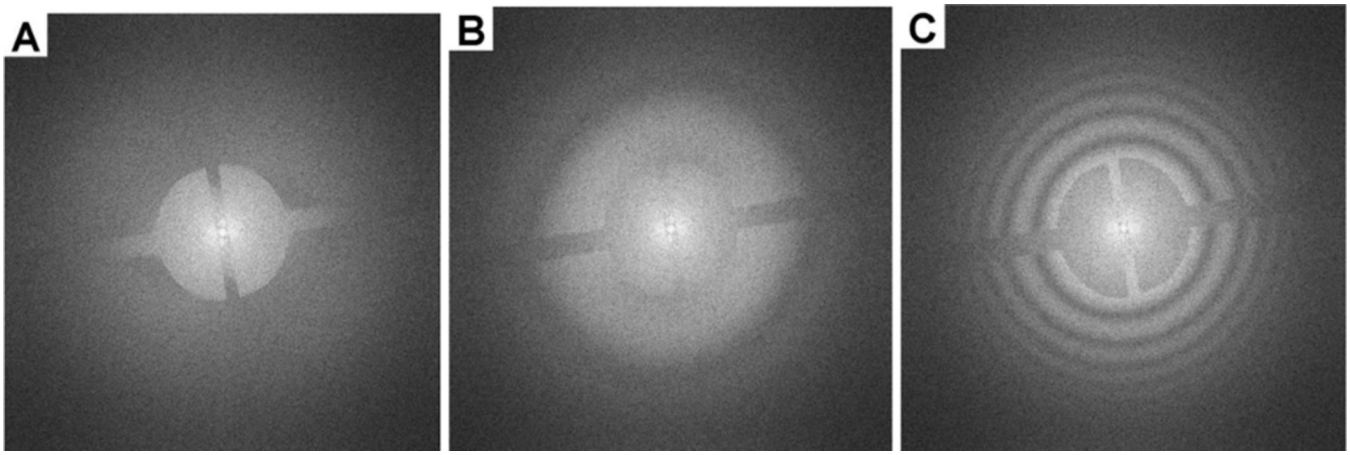

Figure 2.
Fourier transforms from a focal series of images of amorphous carbon film recorded with a hybrid dsb/ssb aperture. (A) Image recorded very close to zero defocus. (B) Image recorded with an underfocus of ~140 nm. (C) Image recorded with an underfocus of ~480 nm. These Fourier transforms illustrate the point that the magnitude of the CTF is constant in the area "behind" the opaque half circle of the hybrid dsb/ssb aperture, while the normal (i.e. dsb) CTF remains at a radius larger than that of the opaque half circle. These Fourier transforms also show that the magnitude of the CTF at the edge of the opaque semicircle of the ssb aperture can be matched by the dsb CTF for the correctly chosen value of defocus (panel B).

NIH-PA Author Manuscript
NIH-PA Author Manuscript
NIH-PA Author Manuscript

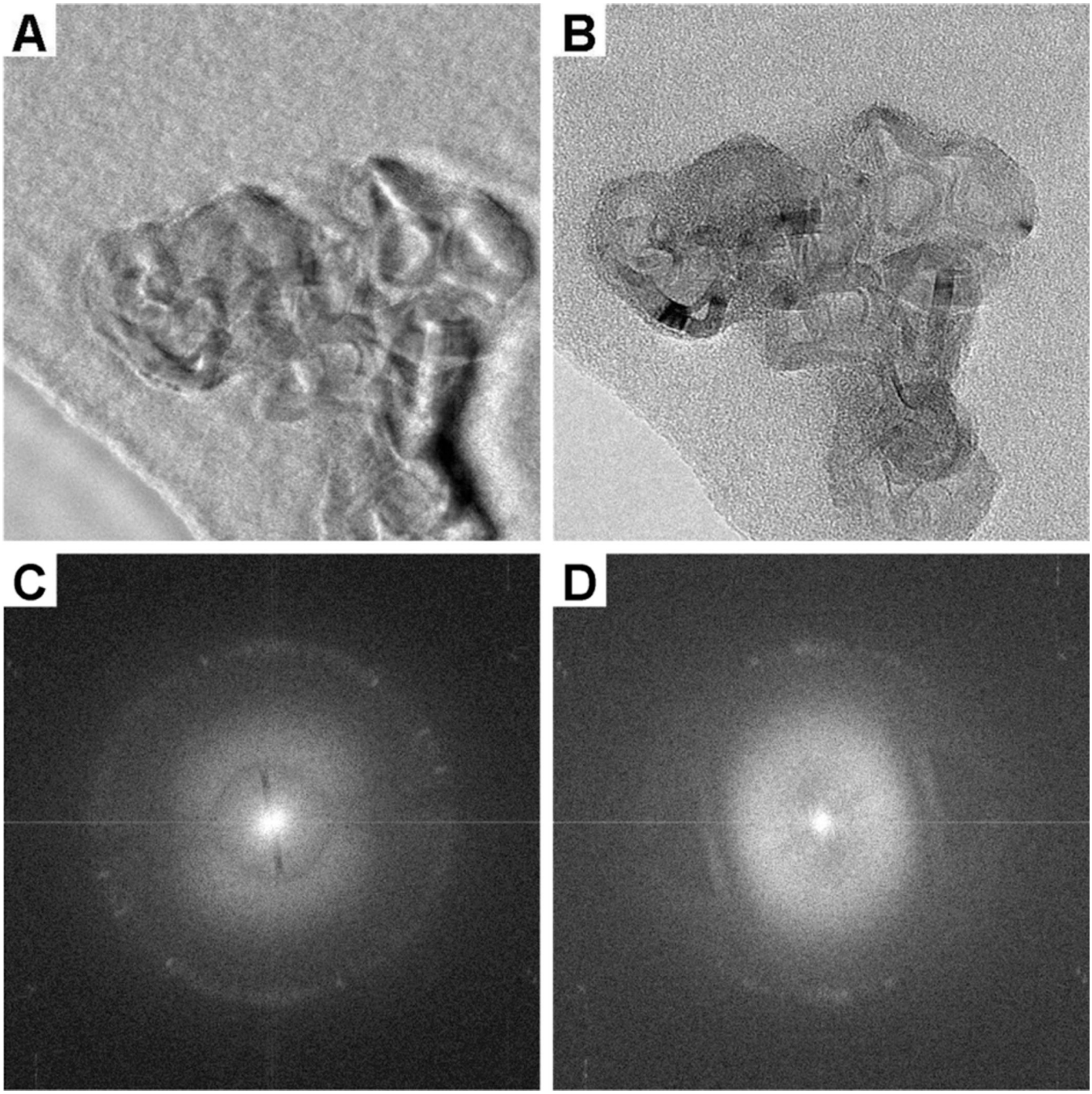

Figure 3.

Images (and their Fourier transforms) of a graphitic particle that were recorded with a hybrid dsb/ssb aperture positioned (A) with the straight edge close to the unscattered electron beam and (B) with the device pulled back such the straight edge is located approximately half way between the unscattered beam and the diffraction ring from the 3.4A spacing of graphite. The pixel size of the CCD camera is 24 μm, and the image magnification at the camera is 220,000. The image recorded with the hybrid aperture (panel A) shows increased contrast relative to the image recorded with the aperture removed a considerable distance from the center of the electron diffraction pattern (panel B). The Fourier transform (panel C) of the image in panel A, recorded with the device centered in the intended way, demonstrates that

NIH-PA Author Manuscript

NIH-PA Author Manuscript

NIH-PA Author Manuscript

signal is well preserved at a resolution of 0.34 nm when using the ssb aperture. The Fourier transform (panel D) of the image in panel B, which was recorded with the device shifted well off center, nevertheless demonstrates that there still is a small amount of charging. Charging is evidenced by the bright line in the FFT at the edge of the aperture and by the distorted shape of the first Thon ring.

NIH-PA Author Manuscript
NIH-PA Author Manuscript
NIH-PA Author Manuscript

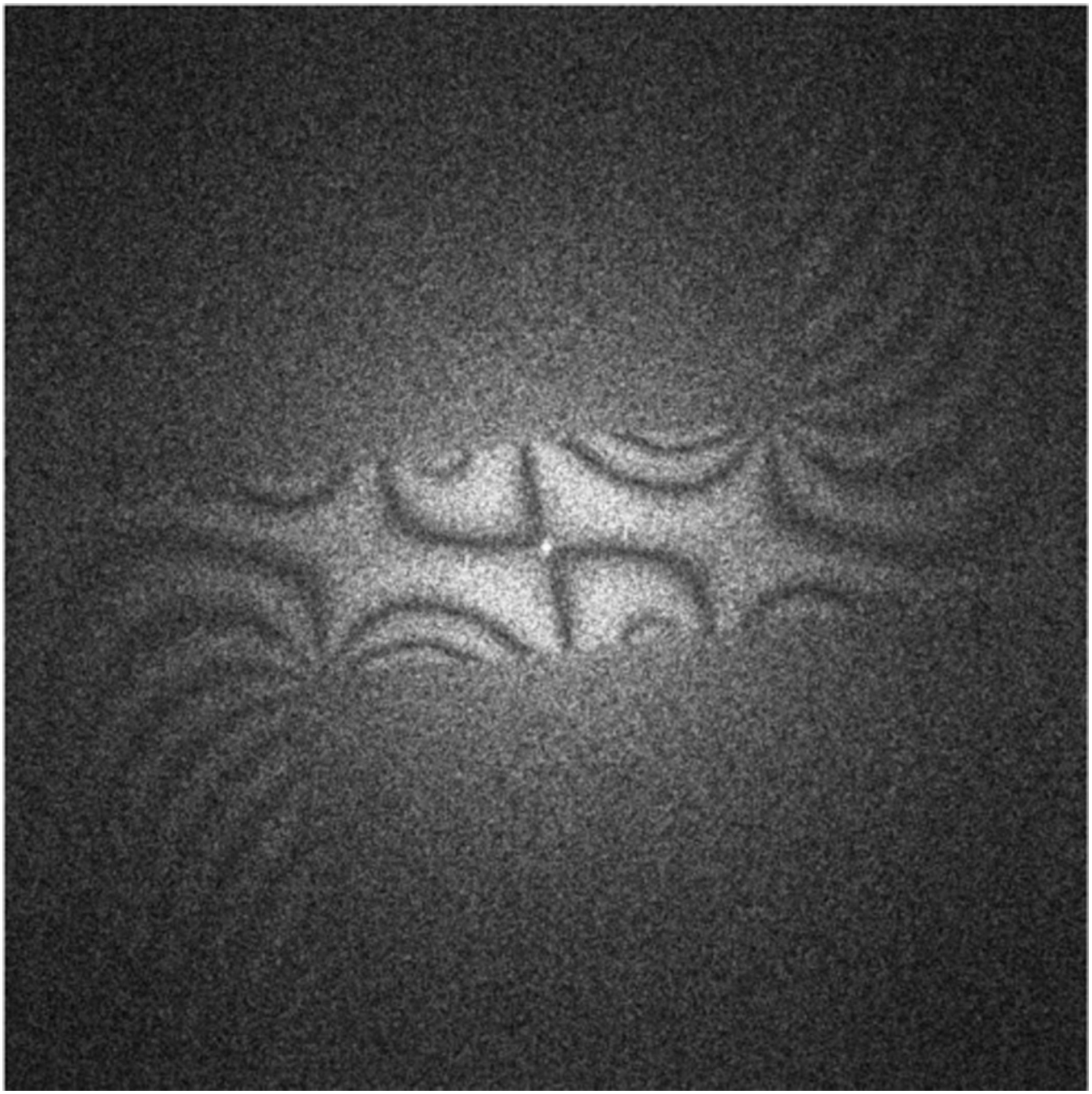

Figure 4.
Representative example of the amount of distortion of the CTF that is caused by charging of the opaque portion of a hybrid dsb/ssb aperture. The test device was, in this case, simply a rectangular strip that extended from one edge to the center of a circular aperture. This device was fabricated from a 25 μm-thick foil of 5N gold, heated to a temperature of 185° C during use in an attempt to prevent the build up of hydrocarbon contamination when hit by the electron beam. The unintended result of heating the device was, as is shown here, that strong phase distortions developed along the entire front edge of the device, unlike the localized phase distortions that occur when the edge of a device is intentionally allowed to be hit (at

room temperature) for 10s of seconds by the unscattered beam of the electron diffraction pattern.

NIH-PA Author Manuscript
NIH-PA Author Manuscript
NIH-PA Author Manuscript